THE ASTROPHYSICAL JOURNAL, 404:678–685, 1993 February 20

SMOOTHED PARTICLE HYDRODYNAMICS NEAR A BLACK HOLE

PABLO LAGUNA,[1,2] WARNER A. MILLER,[1,3] AND WOJCIECH H. ZUREK[1]
Received 1992 June 1; accepted 1992 August 20

ABSTRACT

We derive the smoothed particle hydrodynamic equations for a relativistic fluid in a static curved spacetime geometry. We apply this technique to develop a three-dimensional numerical code for the study of fluid flows around black holes. We present here three one-dimensional benchmarks used in the calibration of our code: (1) relativistic shock tubes, (2) dust infall onto a black hole, and (3) Bondi collapse. Moreover, we describe briefly the use of this computational tool to analyze the tidal disruption of stars by supermassive black holes.

Subject headings: black hole physics — hydrodynamics — methods: numerical — relativity

1. INTRODUCTION

Numerical simulations of fluid flows in the vicinity of strongly gravitating compact objects require a three-dimensional description because of their complex nature and lack of symmetry. An optimal numerical technique should be capable of investing most of the available computational resources (memory and CPU) on domains where the fluid is densest and evolves most rapidly. In other words, computations should proceed with a high degree of spatial refinement and time adaptability. Tidal disruption of stars by black holes (Carter & Luminet 1982; Evans & Kochanek 1989), nonaxisymmetric instabilities of accretion flows (Papaloizou & Pringle 1984; Zurek & Benz 1986), and star-star collisions (Benz & Hills 1987) are examples of physical phenomena that require these features for their numerical simulation. Thus, it is desirable that the available finite number of computational nodes or grid points follow the fluid (Lagrangian description). The Smoothed Particle Hydrodynamics (SPH) discretization approach satisfies these criteria (Gingold & Monoghan 1977).

SPH has become a useful computational tool for complex three-dimensional problems (Benz 1990), and it owes its popularity mostly to its computational simplicity. SPH has been used primarily to study nonrelativistic fluid flows. However, Monaghan & Lahy (1988) derived SPH equations for relativistic fluids moving in a static metric. Recently Kheyfets, Miller, & Zurek (1990) developed a formulation of SPH compatible with the principles of general relativity in which the contact interactions are modeled by spatial smoothing functions constructed explicitly in the local frame comoving with the fluid. Mann (1991) also applied the SPH method to the formulation of Arnowitt, Deser, & Misner 1962, hereafter ADM) of the equations for special-relativistic fluid flows in one dimension. We have taken the next logical step in the progression and applied the SPH techniques in developing a computational tool to study the three-dimensional dynamics of a relativistic ideal fluid in a static curved spacetime geometry.

To what extent does a fluid flow alter the curvature of a background spacetime? What is the domain of applicability of our computer model? A detailed answer to these questions is problem dependent. Nevertheless, our code is valid when (1) the background spacetime is static, and (2) the density of mass-energy of the fluid is sufficiently small that a Newtonian model of the fluid's self-gravity is an adequate approximation.

We have chosen to solve the fluid equations using SPH (Lucy 1977; Gingold & Monaghan 1977) primarily for two reasons: (1) the method bypasses the need of a grid to compute spatial derivatives, avoiding mesh tangling and distortion; and (2) its Lagrangian nature mimics an "adaptive mesh" finite-difference method. However, SPH has its own drawbacks. Boundary conditions in SPH often require a more involved treatment than in the finite-difference methods. Therefore, SPH is easiest to apply to astrophysical systems such as gravitationally bound compact objects whose boundaries are naturally modeled by the decrease of the number of particles as the physical boundary is reached, thus avoiding this difficulty. Another limitation of SPH appears when one models systems with extremely different characteristic lengths or in handling properly material interfaces. Nevertheless, we feel that the computational advantage gained with a mesh-free algorithm such as SPH is essential if we are to make headway in solving the general relativistic equations.

The main goal of this paper is to present our SPH approach to fluid flows in the vicinity of black holes. We have used this method in the development of a three-dimensional numerical code to study tidal stellar disruptions by supermassive black holes (Laguna, Miller, & Zurek 1991; Laguna et al. 1992). A summary of the ADM equations is given in § 2. The methodology of SPH in curved spacetimes is presented in § 3. One dimensional code tests are given in § 4. Finally, conclusions and future applications are discussed in § 5. We use geometric units in which $G = c = k = 1$, where G is the gravitational constant, c is the speed of light, and k is Boltzmann's constant. All of our measurements are given in black hole mass units. Greek (α, β, γ) and Latin (i, j, k) indices are spacetime and spatial indices, respectively. Latin (a, b, c) indices label particles.

2. THE CONTINUUM HYDRODYNAMIC EQUATIONS

The variables that completely characterize the fluid under our consideration are the four-velocity U^μ of an observer comoving with the fluid, the baryon rest mass density ρ, the specific internal energy ϵ, and the isotropic pressure P. Other useful quantities are the energy density $\rho\epsilon$ and the total inertial-carrying energy density ρh, with $h = 1 + \epsilon + P/\rho$ the relativistic enthalpy.

[1] Theoretical Astrophysics Group, T-6, MS B288, Los Alamos National Laboratory, Los Alamos, NM 87545.
[2] Department of Astronomy and Astrophysics, The Pennsylvania State University, University Park, PA 16802.
[3] Phillips Laboratory, Kirtland Air Force Base, NM 87117.

Following the ADM formalism of general relativity (Arnowitt et al. 1962), the spacetime line element can be written as

$$ds^2 = -\alpha^2 dt^2 + \eta_{ij}(dx^i + \beta^i dt)(dx^j + \beta^j dt) , \quad (2.1)$$

where α is the lapse function, β^i the shift vector and η_{ij} the spatial metric, $\sqrt{-g} = \alpha\sqrt{\eta}$. As mentioned before, we only consider fixed background spacetime. That is, the metric (2.1) is static, and hence α, β^i, and η_{ij} do not depend on time. In the derivation of the hydrodynamic equations, we follow a procedure similar to the one used by Hawley, Smarr, & Wilson (1984, hereafter HSW). We define the relativistic gamma as

$$\gamma = \left(1 - \frac{V^i V_i}{\alpha^2}\right)^{-1/2} , \quad (2.2)$$

where V^i is the transport velocity defined as

$$V^i = \frac{\alpha}{\gamma} U^i . \quad (2.3)$$

Let us now introduce the equations which determine the evolution of the fluid. The first equation is obtained from the normalization of the four-velocity, $U^\mu U_\mu = 1$. There are in addition two conservation laws: The conservation of baryon number, $\nabla_\mu(\rho U^\mu) = 0$, and the conservation of energy momentum, $\nabla_\mu T^{\mu\nu} = 0$. We are only going to consider perfect fluids; that is, fluids for which the molecular viscosity is ignored, so entropy is conserved along the fluid lines. The stress-energy tensor in this case reads

$$T_{\mu\nu} = \rho h U_\mu U_\nu + P g_{\mu\nu} . \quad (2.4)$$

To properly model jump discontinuities in the hydrodynamical variables, we have introduced an artificial viscosity; hence, entropy will no longer be conserved in applications in which shocks are present.

We now proceed to derive the hydrodynamic equations in a form suitable for SPH discretization. Using equation (2.3), the equation of baryon conservation can be written as

$$\nabla_\mu(\rho\gamma V^\mu/\alpha) = 0 . \quad (2.5)$$

We define the redshifted energy density $D \equiv \rho\gamma$. In addition, the operator $V^\mu\nabla_\mu$, when applied to scalar functions, yields the Lagrangian time derivative d/dt. Equation (2.5) can then be rewritten as

$$\frac{d}{dt} D + D\nabla_i V^i = 0 . \quad (2.6)$$

Using the stress-energy tensor (2.4), the energy conservation equation for a perfect fluid is given by

$$U^\nu[\nabla_\mu(\rho h U^\mu U_\nu) + \nabla_\nu P] = 0 . \quad (2.7)$$

Baryon conservation allows us to rewrite equation (2.7) as

$$\rho U^\mu \nabla_\mu \epsilon + P\nabla_\mu U^\mu = 0 . \quad (2.8)$$

We again use equation (2.3) to obtain from equation (2.8)

$$\frac{d}{dt}\epsilon = -\frac{P}{D}\left(\gamma\nabla_i V^i + \frac{d}{dt}\gamma\right) . \quad (2.9)$$

Finally, from the divergence of the stress-energy tensor (2.4) one obtains

$$\nabla_\mu(\rho h U^\mu U_\nu) + \nabla_\nu P = 0 . \quad (2.10)$$

Using again the baryon conservation equation and examining only the spatial components, the momentum equation can be reexpressed as follows:

$$\frac{d}{dt} S_i + \frac{1}{2}\frac{\alpha}{h\gamma} S_\mu S_\nu \partial_i g^{\mu\nu} = -\frac{\alpha}{D}\nabla_i P , \quad (2.11)$$

where $S_i \equiv h\gamma V_i/\alpha$. Our momentum variable S_i is not the same as the one introduced by HSW; they use $S_i \equiv Dh\gamma V_i/\alpha$ which is more convenient in Eulerian descriptions.

To close the system of equations and unknowns, we need to introduce an equation of state. In the examples discussed below, we shall use the ideal gas equation of state $P = \epsilon\rho(\Gamma - 1)$, where Γ is the ideal gas adiabatic exponent. In terms of our variables this equation of state reads

$$P = \epsilon D(\Gamma - 1)/\gamma . \quad (2.12)$$

The six equations (2.6), (2.9), (2.11), and (2.12) constitute the complete set of equations for the six hydrodynamic variables D, ϵ, S_i, and P.

3. THE SPH EQUATIONS

In the previous section we derived the hydrodynamic equations for a static curved spacetime. The next step is to obtain their SPH discretized representation. Given a function $f(\boldsymbol{x})$, its mean smoothed value can be obtained from

$$\langle f(\boldsymbol{x})\rangle = \int W(\boldsymbol{x}, \boldsymbol{x}'; h) f(\boldsymbol{x}')\sqrt{\eta'} d^3x' , \quad (3.1)$$

where W is the kernel with smoothing length h, and $\sqrt{\eta'}d^3x'$ is the volume element. For consistency, one needs to impose a normalization condition on W:

$$\int W(\boldsymbol{x}, \boldsymbol{x}'; h)\sqrt{\eta} d^3x = 1 . \quad (3.2)$$

Since the volume integral (3.2) is over curved spacetimes, the normalization condition is not as straightforward as it is in flat spacetimes. Here is where one of the important modifications to the standard SPH approach must be introduced. We assume that

$$W(\boldsymbol{x}, \boldsymbol{x}'; h) = K(\boldsymbol{x})\omega(v) , \quad (3.3)$$

where $\omega(v)$ is the spherical spline (flat space) kernel (Monaghan & Lattanzio 1985)

$$\omega(v) = \frac{1}{\pi h^3}\begin{cases} 1 - \frac{3}{2}v^2 + \frac{3}{4}v^3 & (0 \le v \le 1) \\ \frac{1}{4}(2 - v)^3 & (1 \le v \le 2) , \\ 0 & (2 \le v) \end{cases} \quad (3.4)$$

with $v = |\boldsymbol{x} - \boldsymbol{x}'|/h$, and $K(\boldsymbol{x})$ a normalization function. Here we used the fact that spacetime is locally flat, and that the scales of the hydrodynamic variations are (1) sufficiently large compared to the smoothing length, yet (2) much smaller than the radius of curvature of spacetime. It is not difficult to show that, by construction, $\int \omega(v)\sqrt{f} d^3x = 1$, with f the flat space determinant. Therefore, if we choose $K = \sqrt{f/\eta}$, we satisfy the normalization condition (3.2). In the case of a Schwarzschild black hole, $K = \alpha = \sqrt{1 - 2M/r}$.

If the values of the function $f(\boldsymbol{x})$ are known only at a finite

number of discrete points N, we can introduce the number density distribution (Benz 1990)

$$\langle n(\boldsymbol{x})\rangle \equiv \sum_{a=1}^{N} \eta^{-1/2}\delta(\boldsymbol{x}-\boldsymbol{x}_a)\,. \tag{3.5}$$

Substitution of equation (3.5) into equation (3.1) yields

$$\langle f(\boldsymbol{x}_a)\rangle = \sum_{b=1}^{N} \frac{f(\boldsymbol{x}_b)}{\langle n(\boldsymbol{x}_b)\rangle} W(\boldsymbol{x}_a, \boldsymbol{x}_b; h)\,. \tag{3.6}$$

One can show that the following property is also true:

$$< f(\boldsymbol{x})/g(\boldsymbol{x})> = \langle f(\boldsymbol{x})\rangle/\langle g(\boldsymbol{x})\rangle + O(h^2)\,. \tag{3.7}$$

As mentioned before, SPH is an attractive computational tool because it avoids the use of a grid when computing spatial gradients. By definition (3.1), one estimates the smooth value of the gradient of a scalar function as

$$\langle \nabla f(\boldsymbol{x})\rangle = \int W(\boldsymbol{x}, \boldsymbol{x}'; h)\nabla' f(\boldsymbol{x}')\sqrt{\eta'}d^3x'\,.$$

Ignoring surface terms, integration by parts and substitution of $W = K\omega$ gives

$$\langle \nabla f(\boldsymbol{x})\rangle = -\int f(\boldsymbol{x}')[K(\boldsymbol{x}')\nabla'\omega(v) + \omega(v)\nabla' K(\boldsymbol{x}')]\sqrt{\eta'}d^3x'\,.$$

Since the flat kernel ω is spherical, $\nabla'\omega(\boldsymbol{x}, \boldsymbol{x}'; h) = -\nabla\omega(\boldsymbol{x}, \boldsymbol{x}'; h)$; the above expression can then be rewritten as

$$\langle \nabla f(\boldsymbol{x})\rangle = \nabla \int f(\boldsymbol{x}')W(\boldsymbol{x}, \boldsymbol{x}'; h)\sqrt{\eta'}d^3x' - \int f(\boldsymbol{x}')W(\boldsymbol{x}, \boldsymbol{x}'; h)\nabla' \ln K(\boldsymbol{x}')\sqrt{\eta'}d^3x'\,;$$

that is,

$$\langle \nabla f(\boldsymbol{x})\rangle = \nabla\langle f(\boldsymbol{x})\rangle - \langle f(\boldsymbol{x})\rangle\nabla \ln K(\boldsymbol{x})\,. \tag{3.8}$$

A discrete form of this expression is obtained in a manner similar to that used to derive equation (3.6), resulting in

$$\langle \nabla f(\boldsymbol{x}_a)\rangle = \sum_{b=1}^{N} \frac{f(\boldsymbol{x}_b)}{\langle n(\boldsymbol{x}_b)\rangle} \nabla_{\boldsymbol{x}_a} W(\boldsymbol{x}_a, \boldsymbol{x}_b; h) - f(\boldsymbol{x}_a)\nabla_{\boldsymbol{x}_a} \ln K(\boldsymbol{x}_a)\,. \tag{3.9}$$

Similarly, one can show that the divergence of a vector is computed from

$$\langle \nabla\cdot \boldsymbol{A}(\boldsymbol{x})\rangle = \nabla\cdot\langle \boldsymbol{A}(\boldsymbol{x})\rangle - \langle \boldsymbol{A}(\boldsymbol{x})\rangle\cdot\nabla \ln K(\boldsymbol{x})\,, \tag{3.10}$$

and its discrete version is given by

$$\langle \nabla\cdot \boldsymbol{A}(\boldsymbol{x}_a)\rangle = \sum_{b=1}^{N} \frac{\boldsymbol{A}(\boldsymbol{x}_b)}{\langle n(\boldsymbol{x}_b)\rangle}\cdot\nabla_{\boldsymbol{x}_a} W(\boldsymbol{x}_a, \boldsymbol{x}_b; h) - \boldsymbol{A}(\boldsymbol{x}_a)\cdot\nabla_{\boldsymbol{x}_a} \ln K(\boldsymbol{x}_a)\,. \tag{3.11}$$

With properties (3.7), (3.8), and (3.10), we can now derive the SPH version of the ADM hydrodynamic equations. We rewrite the number density distribution of a particle a as $\langle n(\boldsymbol{x}_a)\rangle = D(\boldsymbol{x}_a)/m_a$, where m_a is the rest mass of the fluid particle. From equation (3.6), the baryon mass density is then given by

$$D_a = \sum_{b=1}^{N} m_b W_{ab}\,, \tag{3.12}$$

where $W_{ab} \equiv W(\boldsymbol{x}_a, \boldsymbol{x}_b; h)$. This equation states that the density depends only on the location of the particles and their smoothed mass in space according to the kernel W_{ab}. We use equation (3.12) to compute the density since it satisfies automatically the continuity equation (2.6) when the masses of the particles are constant.

Applying the smoothing equation (3.1) to the energy conservation equation (2.9) yields

$$\left\langle \frac{d}{dt}\epsilon \right\rangle = -\left\langle \frac{P}{D}\left\{\frac{\gamma}{D}\left[\nabla\cdot(D\boldsymbol{V}) - \boldsymbol{V}\cdot\nabla D\right] + \frac{d}{dt}\gamma\right\}\right\rangle\,, \tag{3.13}$$

where we have used $[\nabla\cdot(D\boldsymbol{V}) - \boldsymbol{V}\nabla\cdot D]/D$ instead of $\nabla\cdot\boldsymbol{V}$ because it is more accurate and, in particular, gives the correct result when the velocity is constant. From properties (3.7), (3.8), and (3.10), we obtain

$$\frac{d}{dt}\langle\epsilon\rangle = -\frac{\langle P\rangle}{\langle D\rangle}\left[\frac{\langle\gamma\rangle}{\langle D\rangle}(\nabla\cdot\langle D\boldsymbol{V}\rangle - \langle\boldsymbol{V}\rangle\cdot\nabla\langle D\rangle) + \frac{d}{dt}\langle\gamma\rangle\right]. \tag{3.14}$$

Using equations (3.6), (3.9), and (3.11), the SPH form of the energy conservation equations is given by

$$\frac{d}{dt}\epsilon_a = -\frac{P_a}{D_a}\left[\frac{\gamma_a}{D_a}\sum_{b=1}^{N} m_b(\boldsymbol{V}_b - \boldsymbol{V}_a)\cdot\nabla_a W_{ab} + \frac{d}{dt}\gamma_a\right], \tag{3.15}$$

where $A_a \equiv \langle A\rangle_a$ and ∇_a denotes gradient with respect to $\boldsymbol{x}_a$. Notice that the time derivative of the relativistic gamma appears in the right-hand side of this equation. The handling of this term presents some difficulty for time-explicit integration. For time-implicit differencing, a correct time centering can be obtained (Norman & Winkler 1983). We used a modified version of "operator splitting" (Wilson 1978) to handle this term. For each time step, we use the terms involving the velocity in the right-hand side of equation (3.15) to update the specific energy density. We use this updated value and the velocity renormalization (2.2) to obtain an updated value of γ. A time derivative of γ is then computed from $(\gamma^{(n+1)} - \gamma^{(n)})/\delta t$, which is used to finally update the specific energy density.

Proceeding in the same way as for the energy conservation equation, it is not difficult to show that the smoothed version of the momentum equation is given by

$$\frac{d}{dt}\langle \boldsymbol{S}\rangle + \left\langle \frac{1}{2}\frac{\alpha}{h\gamma} S_\mu S_\nu \nabla g^{\mu\nu}\right\rangle = -\langle\alpha\rangle \times\left(\nabla\left\langle\frac{P}{D}\right\rangle + \frac{\langle P\rangle}{\langle D\rangle^2}\nabla\langle D\rangle - 2\frac{\langle P\rangle}{\langle D\rangle}\langle\nabla \ln K\rangle\right), \tag{3.16}$$

or equivalently by

$$\frac{d}{dt}\boldsymbol{S}_a + \frac{1}{2}\frac{\alpha_a}{h_a\gamma_a}(S_\mu S_\nu\nabla g^{\mu\nu})_a = -\alpha_a\sum_{b=1}^{N} m_b\left(\frac{P_a}{D_a^2} + \frac{P_b}{D_b^2}\right)\nabla_a W_{ab} + 2\alpha_a\frac{P_a}{D_a}\nabla_a \ln K_a\,. \tag{3.17}$$

Equations (3.12), (3.15), and (3.17) constitute the central set of equations in our numerical code. Following Benz (1984), we apply a second-order Runge-Kutta time integrator with adaptive time step to these equations. In applications involving

shocks, a mechanism for dissipation of kinetic energy into heat is required. For that purpose, artificial viscosity is introduced as a viscous pressure term of the form (Mann 1991):

$$Q_a = D_a \begin{cases} a l_a c_a |\nabla \cdot V_a| + b l_a^2 |\nabla \cdot V_a|^2 & \text{if } \nabla \cdot V_a < 0 \\ 0 & \text{otherwise} , \end{cases} \quad (3.18)$$

where c_a is the sound velocity and l_a is the length scale over which the shock spreads, typically $l_a = 2.5h_a$. The first term in equation (3.18) represents a bulk viscosity and the second the standard von Neumann-Richtmyer (1950) viscosity. We adjust the free parameters a and b, so we obtain the best shock profiles ($a = 1$ and $b = 1.5$). Monaghan & Gingold (1983) have shown that equation (3.18) does not completely damp velocity fluctuations on scales smaller than the smoothing length. However, when applied, for example, to the case of tidal disruption of stars by black holes (Laguna et al. 1992), adding equation (3.18) to each of the pressure terms in the equations has proved to be quite successful. Other implementations of artificial viscosity in relativistic SPH will be explored elsewhere (Laguna & Miller 1992).

The resolving power of SPH can be further enhanced by allowing for adiabatic changes in the smoothing length. A constant smoothing length is analogous to a fixed grid in finite difference codes. It is clear that with a constant smoothing length, one will develop resolution problems when the characteristic length of the problem changes by large amounts. By introducing a smoothing length that varies in position and therefore in time, new terms appear in the equations (Hernquist & Katz 1989). If we assume that the scale over which the smoothing length varies significantly is much smaller than the smoothing length itself, the correction terms due to variable smoothing length are small compared to the physical terms in the equations and can be neglected.

There is not yet an optimal recipe for updating the smoothing length for individual particles. The goal is to find a smoothing length proportional to the local mean interparticle separation. We have used two procedures. Given the smoothing length $h_a^{(n-1)}$ for particle a at time step $n-1$ and the corresponding number of neighbors $N_a^{(n-1)}$, a prediction for $h_a^{(n)}$ is obtained from (Hernquist & Katz 1989)

$$h_a^{(n)} = h_a^{(n-1)} \frac{1}{2} \left[1 + \left(\frac{N_0}{N_a^{(n-1)}} \right) \right] , \quad (3.19)$$

where N_0 is an input parameter. The second procedure is due to Benz (1990) and consists of making the smoothing length smaller where particles come together and larger when they recede from each other. This is accomplished by

$$\frac{d}{dt} h = -\frac{1}{3} \frac{h}{D} \frac{d}{dt} D , \quad (3.20)$$

which is obtained by differentiation of the following scaling law:

$$h = h_0 \left(\frac{D_0}{D} \right)^{1/3} . \quad (3.21)$$

We can then use the equation of baryon conservation to obtain

$$\frac{d}{dt} h = \frac{1}{3} h \nabla \cdot V . \quad (3.22)$$

Equation (3.22) is computationally inexpensive because the divergence of the velocity is already obtained for the energy conservation equation.

A fundamental requirement of any SPH algorithm is that of finding all particles within the smoothing length of the kernel. The naive implementation of this neighbor-finding routine uses a loop over the other $N-1$ particles in the system, comparing each distance to the cutoff radius of the kernel (actually the square of this distance, to avoid the need for the slow square root operation). This is done for each of the N particles in the system, which results in a number of operations which goes like $N(N-1) \sim N^2$ for large N. Since the hydrodynamic operations scale nearly like N, the computational time for N greater than a few thousand is completely dominated by the neighbor finding.

A better method sets up a special data structure which allows neighbors to be identified much more efficiently. One example, which may be used for a one-dimensional calculation, would be to sort the list of ordinates. Then, all neighbors of any selected particle will form a contiguous group around the chosen particle and may be identified with little effort. It should be clear that the time spent sorting the list is made up many times over by the gain in efficiency in locating the proper particles.

In higher dimensions, the proper procedure is not as easy as a simple sort. One suitable method for three dimensions uses a data structure called an "oct-tree" (Salmon & Warren 1992). The oct-tree data structure collects particles into cubical regions called "cells." The cube which contains the entire system is called the "root" The root cell contains eight subcells which represent the subvolumes obtained by dividing each of the dimensions of the root cell in half. The procedure is recursively continued on the subcells, until each cell is either empty, or contains one particle.

The procedure used to identify neighbors is as follows: The location of the root cell is compared to the location of the particle. If the particle is inside (as it always will be for the root cell, but not necessarily for deeper cells), the cell is divided, and the eight daughter cells are examined. If the particle is farther away from the cell than the smoothing length, all particles within that cell are eliminated from consideration (since they all must be farther away than the nearest part of the cell). If a daughter cell consists of only one particle, its distance is tested directly against the smoothing length. Otherwise, the cell is divided again and the same procedure as for the root cell is repeated.

The procedure for construction and search of oct-trees does not perform efficiently on vector supercomputers such as Crays. It ends up being faster to do more operations, since the operations are simple and may be done as a vector operation. However, on other computer architectures such as highly parallel Muptiple-Instruction Multiple-Data (MIMD) hypercubes (such as Intel Delta or Connection Machine 5), oct-tree data structures may be manipulated very efficiently, as has been demonstrated with advanced gravitational N-body algorithms (Salmon & Warren 1992). These machines will likely offer performances well in excess of vector supercomputers for Lagrangian hydrodynamics codes. A somewhat different style of parallel machine is exemplified by the Single-Instruction Multiple-Data (SIMD) computers such as the Connection Machine 2. It is likely that a special construction of the oct-tree data structure which labels each cell with an integer, rather than the conventional use of pointers, will allow an efficient implementation of the oct-tree neighbor-finding routine on these machines.

In our general relativistic SPH code, we have implemented two neighbor-finding algorithms. For workstations like the

Suns, finding the particles within the domain of the kernel is done via an oct-tree routine. In the case of vector supercomputers such as Crays, we have incorporated a sorted list algorithm (D. Shirley 1992, private communication). We are currently developing an oct-tree–based neighbor-finding algorithm which will be running on SIMD parallel supercomputers.

4. CODE TESTS

We now present three tests used to calibrate our three-dimensional relativistic SPH code. Since our goal is to clearly show the correct implementation of SPH for relativistic fluid flows in static curved spacetimes, we concentrated our attention here to one-dimensional problems.

Any newly developed relativistic hydrodynamic code must be benchmarked against analytic solutions which single out the performance of the special relativistic terms in the code. We calibrated our code with the relativistic shock tube problem for that purpose. This test was used by Centrella & Wilson (1984) and HSW for finite difference codes, and by Kheyfets et al. (1990) and Mann (1991) for SPH codes. The original work on the theory of relativistic hydrodynamical shocks is due to Taub (1948). The particular test under consideration consists of two regions of fluid initially having different densities and internal

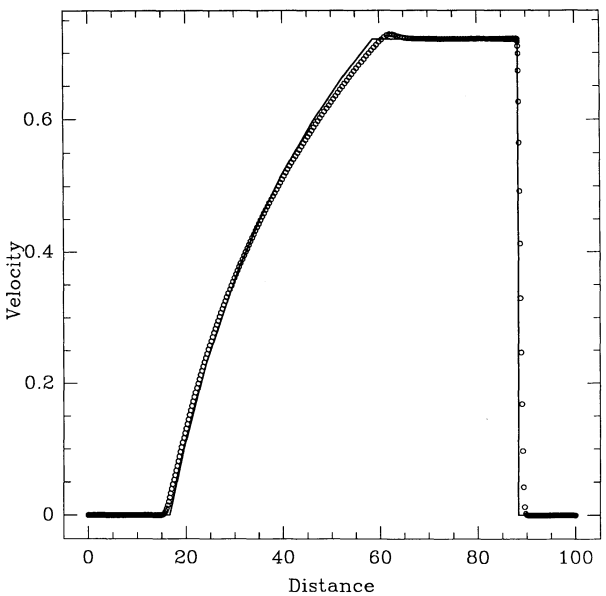

FIG. 1*a*

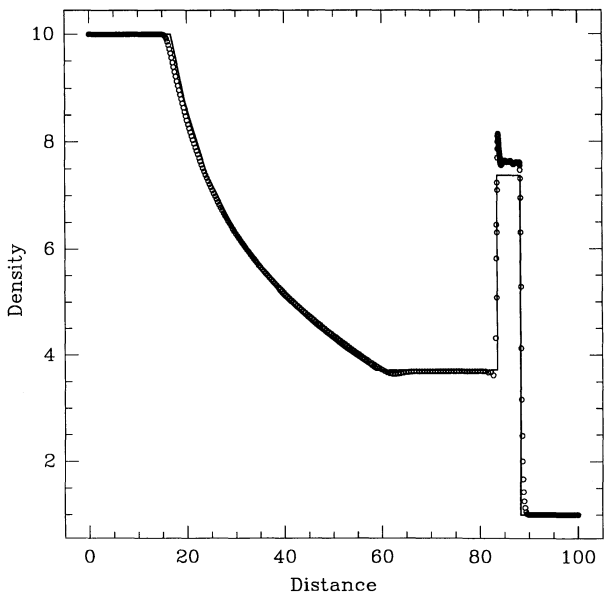

FIG. 1*b*

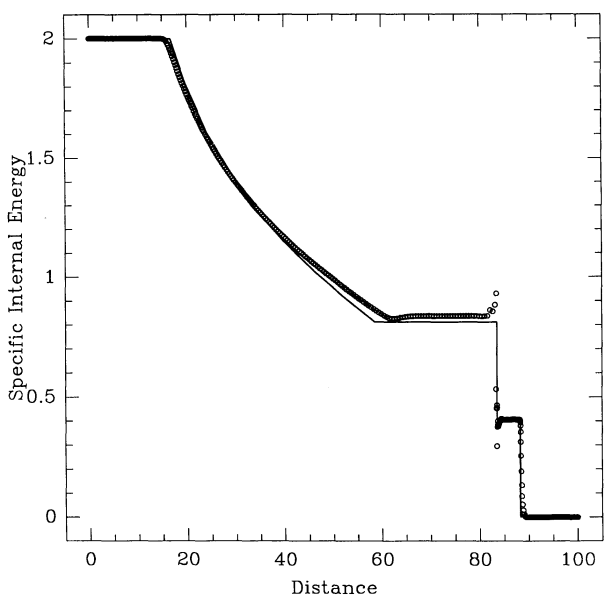

FIG. 1*c*

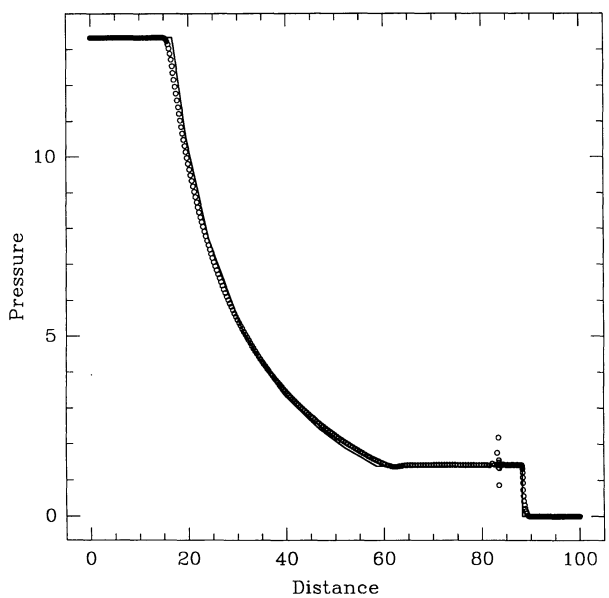

FIG. 1*d*

FIG. 1.—Numerical and analytic solution to the relativistic shock tube with 500 particles for (*a*) velocity, (*b*) density, (*c*) specific internal energy, and (*d*) pressure. The initial conditions to the left of $x = 50$ are $D = 10, \epsilon = 2$, and to the right $D = 1, \epsilon = 10^{-6}$. The intermediate pressure and velocity are $P_m = 1.393$ and $V_m = 0.721$, respectively. The position of the shock and contact discontinuity at $t = 46.5$ are $x_s = 88.3$ and $x_c = 83.5$, with the rarefaction wave extending from $x = 16.7$ to 58.6.

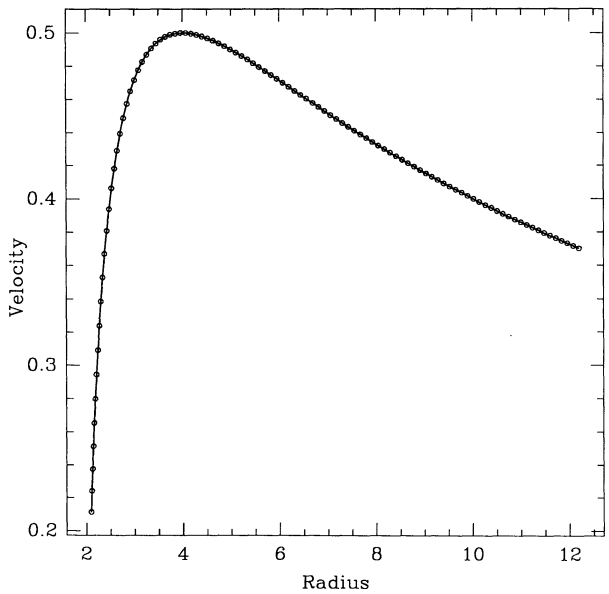

FIG. 2a

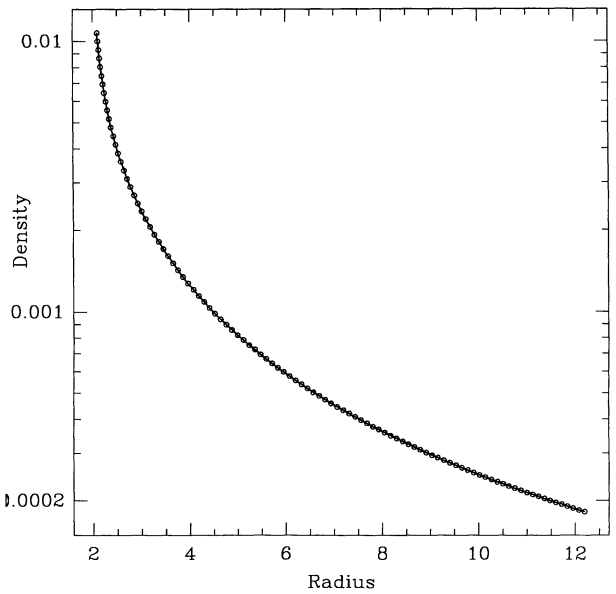

FIG. 2b

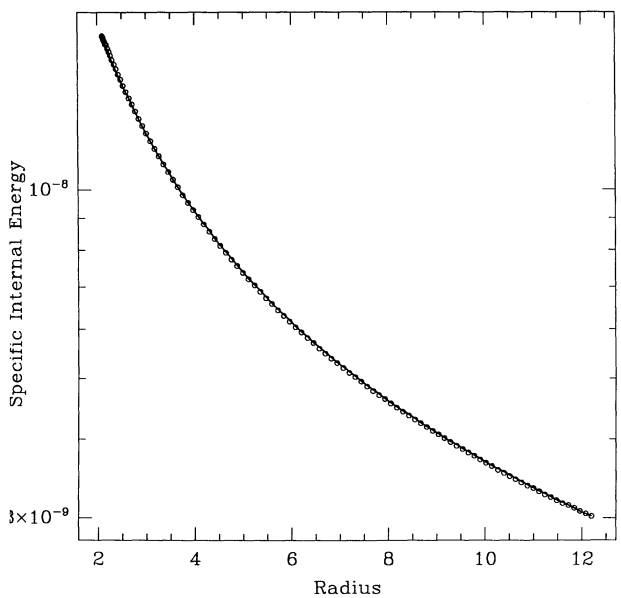

FIG. 2c

FIG. 2.—Numerical and analytic solution to the radial infall of marginally bound dust with 100 particles for (*a*) velocity, (*b*) density, and (*c*) specific internal energy. The accreting fluid follows geodesics, and the binding energy per baryon is conserved.

energies. As the evolution proceeds, a rarefaction wave travels into the denser medium and a compression wave into the lower density fluid. A detailed description of analytic solutions to this test is given by HSW. Figure 1 shows the results of a shock tube with 500 particles. The initial conditions to the left of $x = 50$ are $D = 10$, $\epsilon = 2$, and to the right $D = 1$, $\epsilon = 10^{-6}$. The intermediate pressure and velocity are $P_m = 1.393$ and $V_m = 0.721$, respectively. The position of the shock and contact discontinuity at $t = 46.5$ are $x_s = 88.3$ and $x_c = 83.5$, respectively, with the rarefaction wave extending from $x = 16.7$ to 58.6. Comparison between numerical and analytic solutions is monitored with the maximum relative error among all particles and relative cumulative error over all particles. We find that the maximum relative error occurs in the density (4.1%) at the postshock region of the flow. The largest cumulative error appears on the specific internal energy (2.8%).

The second code test modeled the radial accretion of noninteracting (dust) test fluid particles. This problem was aimed to test the gravitational terms in the equations. The pressure is then negligible. One accomplishes this by initializing the fluid with a small value of the specific internal energy. In this case the elements of the accreting fluid follow geodesics. Once the steady state flow is achieved, the binding energy per baryon hU_t remains constant. One can show (see HSW) that under these assumptions the hydrodynamic variables D, ϵ, and V take the form $V = \alpha\sqrt{1-\alpha^2}$, $D = d_0/r^2V$, and $\epsilon = e_0(D\alpha)^{\Gamma-1}$, with d_0 and e_0 constants of integration. Figure 2 shows the velocity, density, and specific internal energy for a run with 100 particles. The relative cumulative error over all particles is $\lesssim 9.4 \times 10^{-4}$% in the velocity, $\lesssim 7.2 \times 10^{-2}$% in the density, and $\lesssim 0.36$% in the specific internal energy. The maximum relative error over all particles is 1.7×10^{-3}% in the velocity, 0.19% in the density, and 0.72% in the specific internal energy.

The third, and final, test examines the coupling of hydrodynamic terms with gravitational fields. We increase the specific internal energy, and thus the pressure. The fluid elements no longer follow geodesics. The test consists of a continuous, smooth, and steady radial flow onto a black hole. This is a generalization of Bondi accretion in a Schwarzschild metric. Michel (1972) has analytically investigated this problem in full detail. The most important aspect of this problem is the existence of a "critical point." The critical point occurs when the flow goes from a subsonic to a supersonic regime. This point characterizes completely the analytic solution. The code's success in finding such a point demonstrates its accuracy in handling accelerations due to pressure terms. For this purpose, special attention must be paid to boundary conditions. In this test, as well as for dust infall, we have used "ghosts" particles at the boundary. That is, we introduced additional particles whose hydrodynamic values are obtained from the analytic solutions. We have performed a simulation with 100 particles and found (Fig. 3) agreements with the analytic solutions with

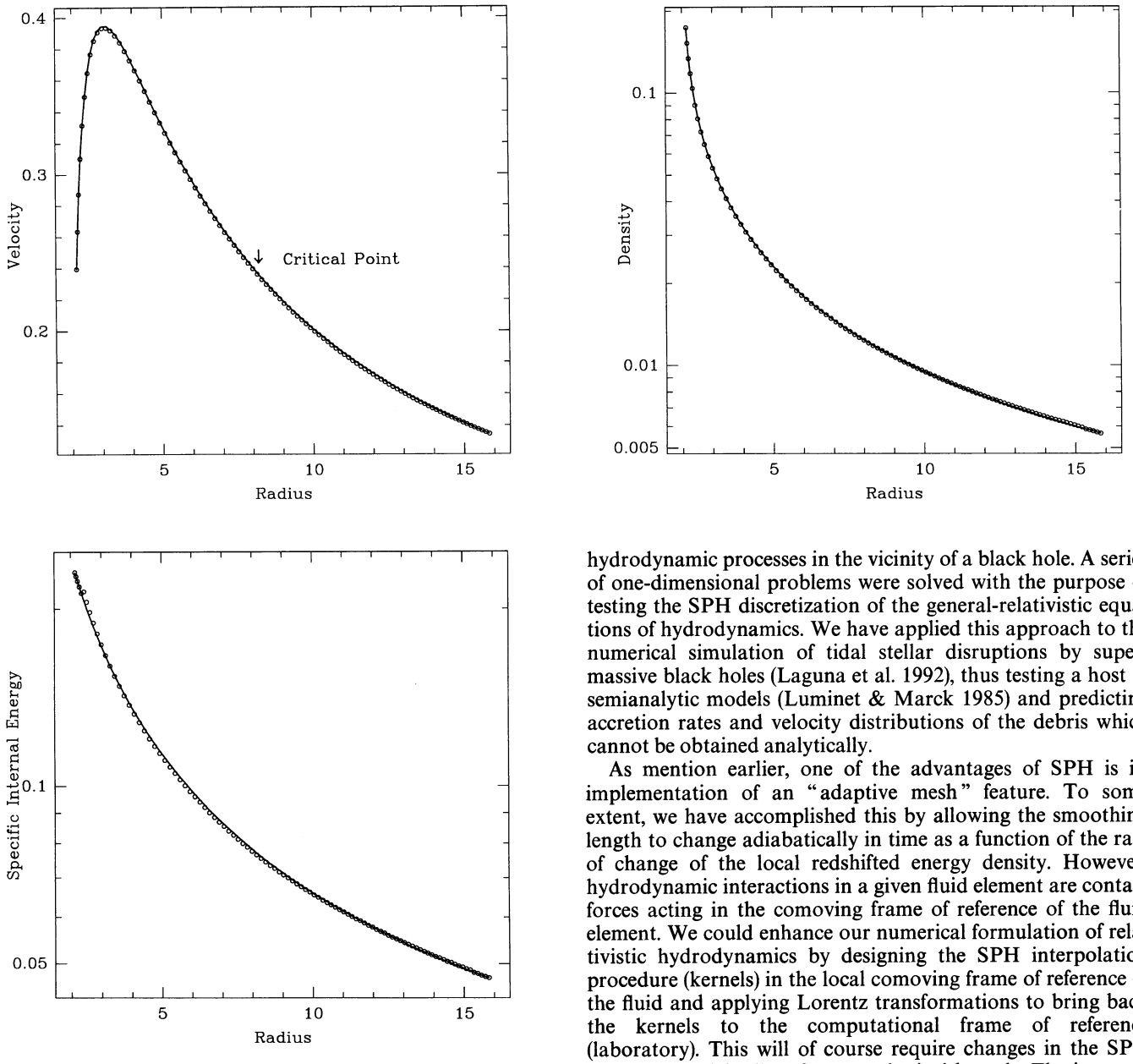

FIG. 3.—Numerical and analytic solution to the Bondi accretion problem with 100 particles for (*a*) velocity, (*b*) density, and (*c*) specific internal energy. The position of the critical point r_c where the fluid goes from a subsonic to a supersonic regime characterizes completely the analytic solution. We have set $r_c = 8$ for the analytic solutions at the boundaries. The error made by the code in finding this point was 1.2%.

cumulative errors $\lesssim 1.1\%$ and maximum relative errors $\lesssim 3.5\%$. We have set the position of the critical point at $r_c = 8$ for the analytic solutions at the boundaries. The error made by the code in finding this point was 1.2%.

5. CONCLUSIONS

We have presented an algorithm based on SPH techniques capable of modeling relativistic fluid flows in static curved spacetimes. We have implemented this algorithm successfully in the development of a three-dimensional code for the study of hydrodynamic processes in the vicinity of a black hole. A series of one-dimensional problems were solved with the purpose of testing the SPH discretization of the general-relativistic equations of hydrodynamics. We have applied this approach to the numerical simulation of tidal stellar disruptions by supermassive black holes (Laguna et al. 1992), thus testing a host of semianalytic models (Luminet & Marck 1985) and predicting accretion rates and velocity distributions of the debris which cannot be obtained analytically.

As mention earlier, one of the advantages of SPH is its implementation of an "adaptive mesh" feature. To some extent, we have accomplished this by allowing the smoothing length to change adiabatically in time as a function of the rate of change of the local redshifted energy density. However, hydrodynamic interactions in a given fluid element are contact forces acting in the comoving frame of reference of the fluid element. We could enhance our numerical formulation of relativistic hydrodynamics by designing the SPH interpolation procedure (kernels) in the local comoving frame of reference of the fluid and applying Lorentz transformations to bring back the kernels to the computational frame of reference (laboratory). This will of course require changes in the SPH equations which allow for nonspherical kernels. The incorporation of nonspherical kernels is not new (Bicknell & Gingold 1983); therefore, we have an indication that this adaptation will present no insurmountable difficulties. We will report on our progress elsewhere (Laguna & Miller 1992). Nevertheless, it is important to realize that most of the relativistic codes to date have a uniform discretization in the laboratory frame, and this introduces a nonisotropic bias inherent to their discretization technique. The ramifications of this issue should be critically examined.

We thank Matt Choptuik, Stirling Colgate, Melvyn Davies, Arkady Kheyfets, and Richard Matzner for numerous discussions. In particular, we thank Mike Warren for his collaboration on implementing an oct-tree neighbor-finding algorithm in our code. Computations were carried out at the Phillips Laboratory Supercomputer Center. This work was performed under AFOSR grant 91NP025.

REFERENCES

Arnowitt, R., Deser, S., & Misner, C. W. 1962, in Gravitation, ed. L. Witten (New York: Wiley), 227 (ADM)
Benz, W. 1984, A&A, 139, 378
———. 1990, in Numerical Modeling of Stellar Pulsation: Problems and Prospects, ed. J. R. Buchler (Dordrecht: Kluwer), 269
Benz, W., & Hills, J. G. 1987, ApJ, 323, 614
Bicknell, G. V., & Gingold, R. A. 1983, ApJ, 273, 749
Carter, B., & Luminet, J. P. 1982, Nature, 296, 377
Centrella, J., & Wilson, J. R. 1984, ApJS, 54, 299
Evans, C. R., & Kochanek, C. S. 1989, ApJ, 346, L13
Gingold, R. A., & Monaghan, J. J. 1977, MNRAS, 181, 32
Hawley, J. F., Smarr, L. L., & Wilson, J. R. 1984, ApJ, 277, 296 (HSW)
Hernquist, L., & Katz, N. 1989, ApJ, 70, 419
Kheyfets, A., Miller, W. A., & Zurek, W. H. 1990, Phys. Rev. D, 41, 451
Laguna, P., & Miller, W. A. 1992, in preparation
Laguna, P., Miller, W. A., & Zurek, W. H. 1991, in Testing the AGN Paradigm, ed. S. S. Holt, S. G. Neff, & C. M. Urry (New York: AIP), 48
Laguna, P., Miller, W. A., Zurek, W. H., & Davies, M. B. 1992, ApJ, submitted
Lucy, L. 1977, AJ, 82, 1013
Luminet, J. P., & Marck, J. A. 1985, MNRAS, 212, 57
Mann, P. J. 1991, Comp. Phys. Comm., 67, 245
Michel, F. C. 1972, Ap&SS, 15, 153
Monaghan, J. J., & Gingold, R. A. 1983, J. Comput. Phys., 52, 374
Monaghan, J. J., & Lahy, N. K. 1988, in Proc. 5th Marcel Grossmann Meeting, ed. D. G. Blair & M. J. Buckingham (Singapore: World Scientific), 1179
Norman, M. L., & Winkler, K. H. 1983, in Radiation Hydrodynamics, ed. M. Norman & K. H. Winkler (Dordrecht: Reidel), 449
Papaloizou, J. C. B., & Pringle, J. E. 1984, MNRAS, 208, 721
Salmon, J., & Warren, M. S. 1992, unpublished
Taub, A. 1948, Phys. Rev., 74, 328
von Neumann, J., & Richtmyer, R. D. 1950, J. Appl. Phys., 21, 232
Wilson, J. R. 1978, in Sources of Gravitational Radiation, ed. L. L. Smarr (Cambridge: Cambridge Univ. Press), 423
Zurek, W. H., & Benz, W. 1986, ApJ, 308, 123